

Accepted for publication in the Astrophysical Journal.

PROBING THE MAGNETIZED INTERSTELLAR MEDIUM SURROUNDING THE PLANETARY NEBULA SH 2-216

R. R. Ransom¹, B. Uyaniker^{1,2}, R. Kothes^{1,3} and T. L. Landecker¹

Ryan.Ransom@nrc-cnrc.gc.ca

ABSTRACT

We present 1420 MHz polarization images of a $2.5^\circ \times 2.5^\circ$ region around the planetary nebula (PN) Sh 2-216. The images are taken from the Canadian Galactic Plane Survey (CGPS). An arc of low polarized intensity (size $0.2^\circ \times 0.7^\circ$) appears prominently in the north-east portion of the visible disk of Sh 2-216, coincident with the optically identified interaction region between the PN and the interstellar medium (ISM). The arc contains structural variations down to the $\sim 1'$ resolution limit in both polarized intensity and polarization angle. Several polarization-angle “knots” appear along the arc. By comparison of the polarization angles at the centers of the knots and the mean polarization angle outside Sh 2-216, we estimate the RM through the knots to be $-43 \pm 10 \text{ rad m}^{-2}$. Using this estimate for the RM and an estimate of the electron density in the shell of Sh 2-216, we derive a line-of-sight magnetic field in the interaction region of $5.0 \pm 2.0 \mu\text{G}$. We believe it more likely the observed magnetic field is interstellar than stellar, though we cannot completely dismiss the latter possibility. We interpret our observations via a simple model which describes the ISM magnetic field around Sh 2-216, and comment on the potential use of old PNe as probes of the magnetized ISM.

Subject headings: planetary nebulae: individual (Sh 2-216) — ISM: structure — polarization — radio continuum: ISM

¹National Research Council of Canada, Herzberg Institute of Astrophysics, Dominion Radio Astrophysical Observatory, Box 248, Penticton, BC, V2A 6J9, Canada

²Present Address: 35-3737 Gellatly Road, Westbank, BC, V2T 2W8, Canada

³Department of Physics and Astronomy, University of Calgary, 2500 University Drive NW, Calgary, AB, T2N 1N4, Canada

1. INTRODUCTION

The diffuse Galactic synchrotron radiation provides a continuous background of radio emission which is intrinsically highly (up to $\approx 70\%$) linearly polarized. This radiation is Faraday-rotated from the point of emission as it propagates through warm ionized gas interwoven with magnetic fields in the disk of the Galaxy; i.e., the angle θ of the polarized component of the emission is rotated at wavelength λ [m] by

$$\Delta\theta = RM \lambda^2 \text{ [rad]}, \quad (1)$$

where RM is the rotation measure [rad m^{-2}] and depends on the line-of-sight component of the magnetic field, B_{\parallel} [μG], the thermal electron density, n_e [cm^{-3}], and the path length, dl [pc], as

$$RM = 0.81 \int B_{\parallel} n_e dl \text{ [rad m}^{-2}\text{]}. \quad (2)$$

High-resolution radio polarization images at frequencies $\lesssim 3$ GHz reveal the turbulent imprint of Faraday rotation on the diffuse polarized emission (e.g., Wieringa et al. 1993; Gray et al. 1999; Gaensler et al. 2001; Uyaniker et al. 2003; Haverkorn, Katgert, & de Bruyn 2003a,b; Haverkorn et al. 2006b; Schnitzeler et al. 2007). The turbulent nature of the imprint is the product of the random component of the Galactic magnetic field and irregular electron-density distributions in the general interstellar medium (ISM). Detailed studies and modeling of the diffuse Galactic emission (e.g., Spoelstra 1984; Haverkorn, Katgert, & de Bruyn 2004a) as well as statistical analyses of the RM s of polarized extragalactic sources (Haverkorn et al. 2006a) indicate that the scale size, or “cell” size, for variations in the magnetized ISM range from ~ 15 pc to 100 pc. Depth depolarization then results from the averaging of nonparallel polarization vectors from emission at different cells along the line-of-sight. Smaller-scale variations are also apparent in polarization images. Depolarization filaments, or “canals,” with a width corresponding to one beam of the observing instrument, indicate the presence of very sharp gradients in RM (see, e.g., Gaensler et al. 2001; Uyaniker et al. 2003; Haverkorn, Katgert, & de Bruyn 2004b). If the gradient is so steep across the beam as to cause differential rotation of the polarization angle of $\sim 90^\circ$, then complete depolarization occurs. Beam depolarization in images produced by aperture synthesis telescopes (typically with arcminute resolution) suggests a scale length for RM structures in the magnetized ISM of less than 1 pc.

Interpreting the structure seen in radio polarization images of the Galactic plane is largely left to modeling (e.g., Haverkorn et al. 2004a), as there is generally little correlation between the polarization structures seen in these images and the emission structures seen in total intensity images. Nevertheless, objects of known distance can be used to estimate the line-of-sight distribution of the magnetized ISM, revealing, for example, whether observed

polarization structures are generated behind the known object, in the region between the object and the Sun, or perhaps in the immediate vicinity of the object (see Gray et al. 1999; Uyaniker & Landecker 2002). Moreover, if small-scale depolarization structures can be isolated to a known object, then it may be possible to probe directly the properties of the magnetized ISM within the structures.

H II regions and supernova remnants (SNRs) are the two most prevalent (discrete) constituents of the ISM as seen at radio wavelengths, and each class of object is detected in radio polarization images up to a limiting distance determined by the “polarization horizon” (see Kothes & Landecker 2004). H II regions are detected by way of their depolarizing effects on background diffuse emission, while SNRs are simultaneously a source of polarized synchrotron emission and a Faraday “screen” which depolarizes background emission. However, neither class of object is a particularly good probe of the magnetized ISM. H II regions have very high electron densities and turbulent motions which produce tangled magnetic fields, a combination which leads to virtually complete beam depolarization across the region. For SNRs, complex models are needed to describe the physical parameters in the shock front at the interface between the rapidly expanding SNR and the ISM.

Another class of object which may potentially serve as a better probe of the magnetized ISM is planetary nebulae (PNe). Young PNe are relatively strong thermal radio emitters, resulting from high electron densities (see, e.g., Bains et al. 2003), but they are also very compact ($\ll 1$ pc) and not yet interacting with the ISM. On the other hand, the shells of many old PNe are observed at optical wavelengths to interact with the ISM (see Tweedy & Kwitter 1996). Moreover, the ISM magnetic field appears to play a significant role in shaping the shells, as evidenced primarily by the visible “striping” or filamentary structure of shell gases (see Tweedy, Martos, & Noriega-Crespo 1995; Soker & Zucker 1997). Theoretical treatments show that interactions between PNe and the ISM are an important consideration in the evolution of PN systems moving at even modest speeds ($\gtrsim 5$ km s $^{-1}$) with respect to the ISM (see, e.g., Soker & Dgani 1997; Wareing, Zijlstra, & O’Brien 2007). If the conditions are right in the interaction region between the PN and the ISM, we may expect to see the Faraday signature of old PNe in radio polarization images. Such a signature has been identified for the nearby PN Sharpless 2-216 (Sh 2-216) and was first described by one of us in Uyaniker (2004). In this paper, we describe in detail the Faraday-rotation structure in the shell of Sh 2-216.

We present radio polarization images at 1420 MHz of a $2.5^\circ \times 2.5^\circ$ region of the Galactic plane around the position of Sh 2-216. The images are taken from the Canadian Galactic Plane Survey (CGPS). In § 2, we summarize the pertinent properties of Sh 2-216. In § 3, we describe briefly the preparation of the images. In § 4, we describe the structures observed on

the visible disk of Sh 2-216 in both polarized intensity and polarization angle, and estimate the RM through the shell of Sh 2-216. In § 5, we derive the magnetic field in the shell of Sh 2-216, and interpret the structures and RM s in the context of an interaction between the PN and the ISM. We also discuss the possibility that the observed structures are produced by the stellar field of the host white dwarf or its progenitor. Finally, in § 6, we summarize our conclusions.

2. THE PLANETARY NEBULA SH 2-216

Sh 2-216 is the closest known PN. At a distance of 129 pc (Harris et al. 2007), its 1.7° angular diameter translates to a physical diameter of 3.8 pc, making it also one of the largest and oldest PNe. The most conspicuous feature of Sh 2-216 at optical wavelengths is its bright eastern rim, denoting an interaction between the expanding and moving PN and the ISM. The location of the interaction region¹ appears to be consistent with the observed displacement of the host white dwarf from the center of the PN; i.e., the enhanced emission in this region is a consequence of the additive velocity of the nebular expansion in all directions and the underlying eastward motion of the PN system relative to the ISM. The expansion velocity is very low ($< 4 \text{ km s}^{-1}$; Reynolds 1985), indicating that the ISM pressure (with dynamic, magnetic and cosmic-ray components) is nearly equal to the PN ram pressure. The velocity (on the plane of the sky) of the system relative to the ISM is estimated also to be $\sim 4 \text{ km s}^{-1}$ (Tweedy et al. 1995).

The thin filamentary structures observed in $H\alpha$ in the interaction region, together with the more subtle, and wider, filamentary structure observed in N II across the face of the PN, qualitatively suggest that the ISM magnetic field is shaping the morphology of Sh 2-216 (Tweedy et al. 1995). Using estimates for the electron density within the PN ($n_e \sim 5 \text{ cm}^{-3}$) and the mean ISM magnetic field ($B \sim 5 \mu\text{G}$), Tweedy et al. (1995) show that the ISM magnetic pressure is about twice that of the dynamic pressure, and thus likely a dominant factor in the shaping. The strength of the PN magnetic field is expected to be negligible at large radii ($r \sim 1 \text{ pc}$) from the host white dwarf, assuming the field decreases as $B \sim r^{-2}$ (see, e.g., Vlemmings, Diamond, & van Langevelde 2002), but may be amplified significantly within filaments due to compression (see Soker 2002; Huggins & Manley 2005). We discuss the strength and orientation of the magnetic field in the outermost regions of Sh 2-216 in § 5.

¹We refer to the bright eastern rim as “the interaction region” throughout the paper, though other parts of the shell of Sh 2-216 may also be interacting with the ISM.

3. OBSERVATIONS AND IMAGE PREPARATION

The radio polarization data presented in this paper were obtained at 1420 MHz ($\lambda = 21$ cm) as part of the CGPS (Taylor et al. 2003) using the synthesis telescope (ST) at the Dominion Radio Astrophysical Observatory (DRAO). The ST is described in detail by Landecker et al. (2000). Images are produced in each CGPS field for the two orthogonal linear polarization states, Stokes-Q (Q) and Stokes-U (U), as well as Stokes-I (total intensity), from data in each of four 7.5 MHz continuum bands centered on 1406.65, 1414.15, 1426.65 and 1434.15 MHz, respectively². Images in Stokes-V, nominally representing circular polarization, are presently dominated by instrumental errors, and are of significantly lower value. The DRAO ST is sensitive at 1420 MHz to emission from structures with angular sizes of $\sim 1^\circ$ (corresponding to the shortest, 12.9 m, baseline of the ST) down to the resolution limit of $\sim 1'$ (corresponding to the longest, 617.1 m, baseline). In total intensity, data from the Effelsberg 21-cm Radio Continuum Survey (Reich et al. 1997) are added to the band-averaged ST data to provide information on the largest spatial scales (see Taylor et al. 2003). In Q and U , data from two single-antenna surveys of the northern sky at ~ 1.4 GHz, namely the DRAO-26m survey (Wolleben et al. 2006) and the Effelsberg Medium Latitude Survey, are added to the band-averaged ST data (see Landecker et al. 2008). All CGPS images presented in this paper were produced using band-averaged data.

CGPS data calibration and processing procedures are described in detail in Taylor et al. (2003). Here we summarize for the reader the general practice, emphasizing procedures related specifically to polarization. The complex antenna gains for the pointing centers in each CGPS field are calibrated by observing a compact calibrator source, either 3C 147 or 3C 295, at the start and end of each observing session. The polarization angle is calibrated using the polarization calibrator source 3C 286. Amplitude and phase variations encountered during individual observing sessions (on time scales down to ~ 2 hr) are determined during the processing of the total intensity data, and are applied also to the Q and U data. Additional processing, needed to remove the effects of strong sources both inside and outside the primary beam of the ST antennas, is accomplished using routines developed especially for the DRAO ST (see Willis 1999). The instrumental polarization, which is corrected on-axis in the sequence above, varies across the primary beam of the ST antennas due to cross-polarization of the (nominally orthogonal) receiver feeds and the effects of the feed support struts (see Ng et al. 2005). The result is “leakage” of unpolarized radiation, seen in total intensity, into Q and U . We have employed two different methods at DRAO to correct for

²Note that the frequency corresponding to the midpoint of the four continuum bands is 1420.4 MHz, the neutral hydrogen spin-flip frequency. The 5.0 MHz band about this frequency is allocated to the 256-channel spectrometer (see Taylor et al. 2003)

the wide-field instrumental polarization. Both methods were used to calibrate the various CGPS fields appearing to some degree in the $2.5^\circ \times 2.5^\circ$ region presented in this paper. In the first method, we derived the “average” leakage pattern in Q and U across the primary beam of the ST antennas, and subtracted from each of the Q and U images the “leakage image” for total intensity into Q and U , respectively (see Taylor et al. 2003). In the second (and newer) method, we derived the leakage patterns for each of the ST antennas separately, and subtracted the complex leakage pattern created by each pair of antennas directly from the Q and U visibility data (see Reid et al. 2008). The residual instrumental polarization error after the on-axis and wide-field calibration is similar for each method in each processed field, increasing from $\sim 0.3\%$ root-mean-square (rms) at the field pointing center to $\sim 1\%$ at the field edge ($\rho = 75'$). The rms error is reduced further in the mosaicing process. The newer wide-field correction significantly reduces artifacts in Q and U around bright total-intensity sources (i.e., with flux densities $\gtrsim 100$ mJy). No artifacts are seen above the estimated ~ 0.34 mJy beam $^{-1}$ (~ 0.086 K) noise level in the $2.5^\circ \times 2.5^\circ$ region of the CGPS presented in this paper.

4. RADIO POLARIZATION IMAGES OF PN Sh 2-216

In Figure 1 we show images of the $2.5^\circ \times 2.5^\circ$ region around PN Sh 2-216 in both optical intensity at R-band ($\lambda = 6570$ nm) and total radio intensity at 1420 MHz ($\lambda = 21$ cm). The optical image is taken from the Digitized Sky Survey (DSS) and the radio image from the CGPS. The images are presented in Galactic coordinates and centered on the position of the host white dwarf LS V 46 $^\circ$ 21 ($l = 158.49^\circ$, $b = +0.47^\circ$; see Kerber et al. 2003). Note that the center of the visible disk of Sh 2-216 is offset $\approx 24'$ to the Galactic south-west of the white dwarf (see Tweedy et al. 1995). For the optical image, we adjusted the range of intensities to highlight extended emission. For the total radio intensity image, we removed point sources leaving only extended emission. There is a clear enhancement in both images across much of the face of Sh 2-216, relative to the surroundings, but the enhancement is most intense along the (Galactic) north-eastern rim; i.e., in the interaction region between Sh 2-216 and the ISM. Treating the enhancement in the radio image as thermal emission from the shell of Sh 2-216, we can estimate the thermal electron density in the interaction region of the PN (see § 5).

In Figure 2 we show the polarized intensity ($P = \sqrt{Q^2 + U^2 - (1.2\sigma)^2}$, where the last term gives explicitly the noise bias correction) and polarization angle ($\theta_P = \frac{1}{2} \arctan U/Q$) images at 1420 MHz for the $2.5^\circ \times 2.5^\circ$ region in the CGPS around PN Sh 2-216. The polarization images contain several interesting features on a variety of angular scales. The

most notable feature is a low-polarized-intensity arc $\sim 0.15^\circ$ wide and $\sim 0.7^\circ$ in length, coinciding with the north-east portion of the visible disk of Sh 2-216. The reduced intensity and distinct shape of the arc indicate that its appearance is due to the effects of Faraday rotation: specifically (1) localized beam depolarization within the arc of the background diffuse synchrotron emission, and/or (2) cancellation of the background emission, Faraday-rotated within the arc, by foreground synchrotron emission. For background/foreground cancellation to play a significant role, the polarized foreground emission must be a reasonable percentage of the total polarized emission in the direction of Sh 2-216. Galactic models for synchrotron emission predict for the 129 pc foreground toward Sh 2-216 only ~ 0.06 K at 1420 MHz (e.g., Beuermann, Kanbach, & Berkhuijsen 1985). Even if this emission is highly (i.e., $\sim 70\%$) polarized, we expect just ~ 0.04 K of polarized emission in the foreground; i.e., $\lesssim 10\%$ of the 0.47 ± 0.06 K total polarized emission seen outside the visible disk of Sh 2-216 (and at $b > +0.5^\circ$). We conclude, therefore, that beam depolarization plays a larger role in reducing polarized emission over the arc than background/foreground cancellation. Structural variations observed within the arc in both polarized intensity and polarization angle on angular scales down to the resolution limit ($\sim 1'$) further suggest that beam depolarization is responsible for the appearance of this feature. Since the length and location of the arc are very similar to the optically bright rim denoting the PN-ISM interaction region, it would seem there is a physical connection between the conditions and processes in this region which give rise to enhanced optical emission and those which lead to sharp gradients in RM . We discuss the RM structure within the arc in § 4.1.

Aside from the prominent north-east arc, do we see other signatures of Sh 2-216 in the polarization images? The circle representing the visible disk of Sh 2-216 in Figure 2 draws our attention to two suggestive details in the northern half ($b > +0.5^\circ$) of the images: (1) the appearance of a second low-polarized-intensity “arc” $\sim 0.2^\circ$ wide and $\sim 0.4^\circ$ in length, located in the north-west portion of the visible disk of Sh 2-216; and (2) the increased range of polarization angles on the visible disk of Sh 2-216 compared to the surroundings. The small-scale structural variations in polarization angle within the north-west arc indicate that beam depolarization is responsible to at least a moderate degree for the reduced emission in this feature. If this second arc is indeed associated with Sh 2-216, then the conditions for sharp RM gradients in the shell of the PN may not be confined to the optically-identified interaction region. Moreover, a comparison of the range of polarization angles seen inside the visible disk of Sh 2-216 (-82° to $+27^\circ$, rms $\approx 17^\circ$) with those seen outside (-17° to $+32^\circ$, rms $\approx 6^\circ$) suggests that the conditions for moderate RM s are present throughout the shell of Sh 2-216. We present a simple model for the observed polarization structures on the visible disk of Sh 2-216 in § 5.

In contrast to the smaller-scale structures seen on the visible disk of Sh 2-216 in the

northern half of the images ($b > +0.5^\circ$), the southern half of the images ($b < +0.5^\circ$) is dominated by “bands” of relatively low polarized intensity, 0.1° – 0.3° wide, which stretch approximately east-west across the region. The bands have no counterpart in total intensity. The boundary between north and south is clearly marked in the polarization angle image by a jagged line over which the angle changes very rapidly. On close inspection of the polarized intensity image, this line corresponds to a narrow ($\sim 1'$) channel within the northernmost band of virtually zero polarized emission. Changes in the polarization angle across “cells” $< 3'$ in size are seen, to differing degrees, throughout the bands. The bands appear to be part of a large-scale complex which depolarizes the background diffuse emission, most likely before it reaches the position of Sh 2-216. In the less likely scenario that the complex sits between the Sun and Sh 2-216, any polarization signature imprinted on the background by Sh 2-216 is lost. In either case, the positioning of the bands on the sky south of the north-east arc associated with Sh 2-216, and other apparent features on the northernmost portion of the visible disk of the PN, would seem to be fortuitous.

4.1. Rotation-Measure Structure in the North-East Arc

The polarization angle of the relatively bright emission outside the visible disk of Sh 2-216 (and at $b > +0.5^\circ$) has a mean value of $+7^\circ$ and rms variations of only 6° . Along the prominent north-east arc, the polarization angle is observed to change rapidly across the perimeters of roughly elliptical “knots.” The angle inside the perimeters changes more slowly and, indeed, plateaus at the centers of the knots. In Figure 3 we show a small $0.4^\circ \times 0.4^\circ$ region in polarization angle around the north-east arc and identify eight discrete knots. We define as the center of each knot the position of the pixel showing the maximum clockwise (see below) deviation from the background ($+7^\circ \pm 6^\circ$) value. In Table 1 we give the mean value of the polarization angle in each knot. The mean was estimated over an area corresponding to the area of the resolving beam (10 pixels, see Figure 3), excluding, in the cases of knots 2 and 4, pixels which differed from the 10-pixel mean by more than 2σ . Table 1 shows that the polarization angle of the emission emerging from the knots is rotated significantly with respect to the background emission. The weighted mean polarization angle at the centers of the knots is $+78^\circ \pm 22^\circ$. If we assume that emission with polarization angle $+7^\circ \pm 6^\circ$ is incident on the far side of each knot, and for the moment ignore foreground emission, then the incident emission is Faraday rotated in the knots by $\Delta\theta = -109^\circ \pm 23^\circ$. We infer negative, i.e., clockwise, rotation by tracing polarization angles from the outside edge of the arc to the center of any knot. The trace shows that the polarization angle (first) decreases through negatives values. At five of the eight knot perimeters, the polarization angle jumps from -90° to $+90^\circ$, and then continues to decrease to its center value. Since

foreground emission probably cannot be ignored at the $\sim 10\%$ level, we must estimate the maximum deviation expected in the observed polarization angle if, by chance, the foreground emission is rotated 45° relative to the emission emerging from the knots. (Note that foreground emission rotated 90° relative to the background leads to a maximum reduction in polarized intensity, but no net rotation in polarization angle.) Assuming complete beam depolarization at the perimeters of at least some of the knots, in particular knots 1 and 4, we estimate the polarized foreground emission to be 0.046 ± 0.012 K, consistent with the values predicted by Galactic synchrotron models. Using 0.177 ± 0.044 K for the mean observed (i.e., emerging plus foreground) polarized emission at the centers of the knots (see Table 1), we estimate a maximum deviation of 7° . Adding this in quadrature to the 23° statistical uncertainty gives a standard error for the measured rotation through the knots of 24° . For a center wavelength of 21.12 cm (see § 3), a rotation of $-109^\circ \pm 24^\circ$ gives (via Equation 1) $RM = -43 \pm 10$ rad m $^{-2}$.

The emission emerging from the centers of the knots, where the polarization angles plateau, is likely higher than the 0.177 ± 0.044 K value given above, but polarization-angle variations over the resolving beam lead to reduced polarized intensity even inside the knot perimeters. While these variations are reflected in the range of angles observed in each knot (see Table 1), we nevertheless believe our estimated mean RM reflects a real systematic rotation of the background emission as it passes through the knots. The consistent clockwise rotation of the polarization angle observed in moving from outside the north-east arc toward the center of any knot strengthens this assertion.

We tried to estimate the RM through the knots using the four-band data from the ST but failed. Given the typical uncertainty in polarization angle in the band-averaged image, and noting that $RM \approx -43$ rad m $^{-2}$ gives a difference in rotation angle of only $\sim 5^\circ$ over 27.5 MHz ($\Delta\lambda = 0.41$ cm), the failure is not surprising.

5. DISCUSSION

We can derive the line-of-sight component of the magnetic field through the knots in the north-east arc of Sh 2-216 using -43 ± 10 rad m $^{-2}$ as an estimate of the RM in the knots, and using estimates of the thermal electron density in and path length through the interaction region (see Equation 2). The electron density in Sh 2-216 can be calculated from emission measure ($EM = \int n_e^2 dl$) determinations, made independently at optical and radio wavelengths. Based on their measured H α intensity and gas temperature ($T_e = 9400 \pm 1100$ K), Reynolds (1985) estimates a mean value for the emission measure over Sh 2-216 of $EM \approx 42$ cm $^{-6}$ pc. Using a brightness temperature of $T_b = 0.11 \pm 0.02$ K for the

thermal radio emission in the interaction region of Sh 2-216 (obtained via comparison of on-source and off-source temperatures in Figure 1*b*), and the same gas temperature, we estimate a value for the interaction region of $EM = 69 \pm 13 \text{ cm}^{-6} \text{ pc}$. If we assume for the moment that electrons are uniformly distributed over the approximately spherical volume of Sh 2-216, and use an average path length through the sphere of $\Delta l = \frac{4}{3}R_{\text{PN}} \approx 2.5 \text{ pc}$, then the optically-determined EM gives a mean electron density over Sh 2-216 of $n_e \approx 4.1 \text{ cm}^{-3}$. In some contrast, the radio-intensity-determined EM gives, for a path length³ through the interaction region of $\Delta l = 1.1 \pm 0.3 \text{ pc}$, $n_e = 7.9 \pm 1.3 \text{ cm}^{-3}$. The factor ~ 2 increase in the electron density in the interaction region compared to the mean value over the entire PN is reasonable, since material is stacking up in the interaction region (see Tweedy et al. 1995). However, $n_e = 7.9 \pm 1.3 \text{ cm}^{-3}$ still represents a mean over the interaction region. The $\text{H}\alpha$ images of Tweedy et al. (1995) show small-scale filamentary structures in the interaction region with localized factor 1.5–2 enhancements in EM relative to the mean. The filaments correspond approximately in both location and size to the polarization-angle knots. Since we cannot confirm the physical association between the filaments and the knots, we conservatively assume an EM -enhancement of 1.5 ± 0.5 , and estimate the electron density in the knots to be $n_e = 9.7 \pm 2.3 \text{ cm}^{-3}$. Using $RM = -43 \pm 10 \text{ rad m}^{-2}$, $n_e = 9.7 \pm 2.3 \text{ cm}^{-3}$ and $\Delta l = 1.1 \pm 0.3 \text{ pc}$, we derive a line-of-sight magnetic field through the knots in the interaction region of $B_{\parallel} = 5.0 \pm 2.0 \mu\text{G}$. Since the RM is negative, this field is directed into the plane of the sky.

5.1. An ISM Origin for the Magnetic Field in the Shell of Sh 2-216

Is a $\sim 5 \mu\text{G}$ line-of-sight magnetic field reasonable for the ISM around Sh 2-216? Since there is no direct measurement of the ISM magnetic field around Sh 2-216, we estimate the local field from what is known generally about the Galactic magnetic field. The Galactic magnetic field is concentrated in the disk and has two components (see, e.g., Beck et al. 1996): a large-scale or regular component (B_{reg}), which follows the spiral arms, and a small-scale or random component (B_{ran}). B_{reg} in the local spiral arm is found, using polarized radio sources and the polarization of starlight, to be directed toward $l \approx 85^\circ$ (e.g., Rand & Lyne 1994; Heiles 1996b; Brown & Taylor 2001); i.e., clockwise as viewed from the Galactic north pole. Fluctuation cell sizes for B_{ran} are estimated to be 50–100 pc (see Rand & Kulkarni 1989; Ohno & Shibata 1993). The ratio of the strengths of the random and regular components of the Galactic field, $B_{\text{ran}}/B_{\text{reg}}$, can be obtained directly from

³The path length $\Delta l = 1.1 \pm 0.3 \text{ pc}$ corresponds to the mean of the line-of-sight chord lengths through a 1.9-pc radius sphere at the positions of the eight knots.

starlight polarization data and synchrotron polarization data using the model presented in Burn (1966). The starlight polarization data of Fosalba et al. (2002) give for a large sample of stars covering all Galactic longitudes $B_{ran}/B_{reg} \approx 1.3$. Using stars from the sample of Mathewson & Ford (1970) in the range $120^\circ < l < 180^\circ$, and a modified version of the Burn model, Heiles (1996a) finds $B_{ran}/B_{reg} \approx 1.5$. For synchrotron emission just north of the visible disk of Sh 2-216 ($l = 158.5^\circ$), we measure a fractional linear polarization of $p = 0.27 \pm 0.03$, close to the maximum value found by Spoelstra (1984) for the diffuse emission in the Galactic plane. With a spectral index $\alpha = -0.44 \pm 0.04$ ($S \propto \nu^\alpha$) between 408 MHz and 1420 MHz for the synchrotron emission in the CGPS region around Sh 2-216, we get for the intrinsic value of the fractional linear polarization $p_{max} = 0.68 \pm 0.01$ (see Ginzburg & Syrovatskii 1965), and thus obtain $B_{ran}/B_{reg} = 1.51 \pm 0.13$, consistent with the Heiles (1996a) starlight estimate. Using a value $B_{tot} = 4.2 \mu\text{G}$ for the average azimuthal field strength ($B_{tot}^2 = B_{reg}^2 + B_{ran}^2$) in the local arm (Heiles 1996a) and $B_{ran}/B_{reg} = 1.51$, we estimate $B_{reg} \approx 2.3 \mu\text{G}$ and $B_{ran} \approx 3.5 \mu\text{G}$. The maximum magnetic field at any point in the local arm is then achieved if, by chance alignment, the random field lies parallel to the regular field; i.e., $B_{max} = B_{reg} + B_{ran} \approx 5.8 \mu\text{G}$. At the longitude of Sh 2-216, both the average field ($B_{tot} = 4.2 \mu\text{G}$) and maximum possible field ($B_{max} = 5.8 \mu\text{G}$) lie largely in the plane of the sky, and run from Galactic east to west. The maximum field along the line-of-sight, where $B_{||reg} \approx 0.6 \mu\text{G}$, is $B_{||max} = B_{||reg} + B_{ran} \approx 4.1 \mu\text{G}$, directed into the plane of the sky.

In light of this brief overview, we conclude that an intrinsic $\sim 5 \mu\text{G}$ line-of-sight magnetic field in the ISM at the position of Sh 2-216 is unlikely. Nevertheless, our observations can be used to comment further on the structure of a proposed ISM field in the interaction region as well as other locations in the shell of Sh 2-216. Our estimate of the line-of-sight magnetic field in the interaction region is based on the maximum RM as seen through knots in our polarization angle image. The RM s outside the knots are apparently much lower. The sharp RM gradients over the knot perimeters must be the result of either a rapid change in the electron density or the line-of-sight magnetic field, or both. As we previously noted, the polarization-angle knots appear to be associated with narrow $H\alpha$ filaments observed in the interaction region. The sharp edges of the filaments, which denote a rapid change in EM (and thus electron density), naturally explain RM gradients across knot perimeters. The magnetic field need not change significantly across the interaction region. Realistically, however, the magnetic field is probably affected by turbulence in the hot gas (see § 5.1.1).

If we look west of the north-east arc, toward the center of the visible disk of Sh 2-216, we continue to see polarization angles significantly different from the $+7^\circ \pm 6^\circ$ observed outside the PN (see Figure 2b). Though we don't see prominent structures in this "interior" region, we do see some localized polarization-angle structures. These structures are roughly

coincident with low-level enhancements in $H\alpha$ and $N\ II$ (see Tweedy et al. 1995) and total radio intensity (see Figure 1*b*). Localized electron-density enhancements may therefore be responsible for both the knots in the interaction region and the more extended structures seen across the western portion of the face of Sh 2-216. Indeed, these two apparently different structures may arise from similar underlying structures, seen edge-on in the case of the knots, and face-on in the case of the extended structures (see, e.g., Tweedy et al. 1995). The increased path length through the shell in the interaction region would explain, at least in part, why the EMs and RM s in the filaments/knots are larger than those in the extended structures across the face. A decrease in the line-of-sight component of the magnetic field, moving west from the north-east edge of Sh 2-216 toward the center of the visible disk, could also account for some of the difference (see § 5.1.1).

A second low-polarized-intensity arc appears at the north-west edge of the visible disk of Sh 2-216 (see Figure 2*a*). Small-scale variations in polarization angle within this arc indicate, as in the north-east arc, the presence of sharp RM gradients. However, unlike the north-east arc, there are no plateaus (i.e., multi-pixel regions of roughly constant polarization angle) over which we can confidently estimate some deviation from the outside $+7^\circ \pm 6^\circ$. Consequently, we have no means of estimating the magnitude of the RM through this arc. Nevertheless, there is some indication of the sign of the RM . Moving south from the edge of the north-west arc, the polarization angle (on average) increases, implying positive RM s. To substantiate this finding, we broke the north-west arc into three north-south slices, and used the approach of Wolleben & Reich (2004) to estimate RM together with three other parameters (degree of depolarization, foreground polarized intensity and foreground polarization angle). We found positive RM s for each slice, even when we varied the other parameters away from their “best-fit” values. The positive RM s indicate that the magnetic field in the north-west arc is directed out of the plane of the sky. If the north-west arc is associated with Sh 2-216, and the ISM field is responsible for the observed RM s in both the north-east and north-west arcs, then the intrinsic field must be deflected around the PN.

5.1.1. *A simple model for the ISM magnetic field around Sh 2-216*

For the ISM magnetic field to simultaneously account for the negative RM s observed in the north-east arc and the positive RM s observed in the north-west arc, the intrinsic field must bend significantly around the shell of Sh 2-216 such that it has a $\sim 5\ \mu\text{G}$ line-of-sight component into the sky on the east edge of the PN and a non-zero line-of-sight component out of the sky on the west edge. This is exactly what we might expect in the following scenario (see Figure 4): The intrinsic ISM field around Sh 2-216 is described by the $4.2\ \mu\text{G}$

azimuthal component of the Galactic magnetic field (see Heiles 1996a), which, at $l = 158.5^\circ$, runs in the local arm from Galactic east to west and intersects the plane of the sky at $15.5^\circ \pm 4^\circ$ (Brown & Taylor 2001). The intrinsic field is compressed and deflected by the expanding and moving PN, since it can diffuse only slowly into the partially ionized shell (see Soker & Dgani 1997). The three-dimensional motion of Sh 2-216 is fully characterized by the (Galactic) north-west-directed motion of the host white dwarf (Cudworth & Reynolds 1985; Tweedy et al. 1995) and a line-of-sight motion into the plane of the sky (see below). The motion in the plane of the sky is of less importance for our observations than the motion along the line-of-sight, though the full three-dimensional picture is important for interpreting the alignment of the filaments in the interaction region and wider structures across the face of Sh 2-216 (see Tweedy et al. 1995). At the far side of Sh 2-216, the line-of-sight motion drags the intrinsic field away from the observer. The result is a deflected field around Sh 2-216 which has on the east edge of the PN a line-of-sight component directed into the sky and on the west edge a line-of-sight component directed out of the sky. In the center portion of the PN, the field lies largely in the plane of the sky. The line-of-sight component of the field on the east edge is slightly larger in strength than the intrinsic field itself, while that on the west side is lower. We estimate the line-of-sight motion of Sh 2-216 by consulting the Wisconsin H α Mapper (WHAM) survey (Haffner et al. 2003). The WHAM data show that the H α emission from Sh 2-216 peaks at velocity $+5 \pm 1 \text{ km s}^{-1}$ relative to the local standard of rest. (Note that the sign for velocity is opposite that of RM ; i.e., a positive velocity signifies motion into the plane of sky while a positive RM signifies a magnetic field out of the plane of the sky). The emission surrounding Sh 2-216 peaks at velocities near zero, indicating that the $+5 \pm 1 \text{ km s}^{-1}$ is indeed relative to the surrounding ISM.

The magnetic field described by our model represents only the “smooth” component of the deflected ISM field. The magnetic field in the shell of the PN will also have a turbulent component due to motions in the hot gas. The turbulent component contributes in part to the beam depolarization we observe in the interaction region. The smooth component is responsible for the systematic RM observed through the knots.

5.1.2. *Are old PNe good potential probes of the magnetized ISM?*

We have asked in this section whether or not the magnetic field derived from the observed RM s is reasonable for the ISM around Sh 2-216. If we were, instead, to concede that the derived field is native to the ISM, then we could ask the question: Are old PNe, such as Sh 2-216, good probes of the intrinsic ISM field? The simple qualitative model presented above for Sh 2-216 suggests that we can learn something about the intrinsic field surrounding

this PN. With a more comprehensive (three-dimensional) model of the PN-ISM interaction, it may be possible to work out quite accurately the strength and orientation of the intrinsic field. Since a large percentage of old PNe show PN-ISM interactions similar to Sh 2-216 (see Tweedy & Kwitter 1996), it is perhaps reasonable to assume that the conditions for detectable Faraday rotation are present in the shells of many old PNe in the nearby Galaxy. Given a good model of the interaction in each case, it should then be possible to determine the intrinsic field at many locations.

There are two significant drawbacks to consider before we declare old PNe good potential probes of the magnetized ISM: (1) It may not be possible in many cases to construct a good model of the PN-ISM interaction, due either to large uncertainties in the physical parameters (e.g., ISM and PN particle densities, space velocity of the PN) or to the overall complexity of the interaction. The qualitative model presented above for Sh 2-216 does not comment on either the degree to which the intrinsic field around the PN is compressed or the maximum angle with which the intrinsic field is deflected. Both of these quantities are necessary in order to more accurately determine the intrinsic field from the line-of-sight field. Three-dimensional magneto-hydrodynamic (MHD) simulations can perhaps be used to demonstrate the sensitivity of the intrinsic-field determination to various parameters. (2) The Faraday signature of the PN is at the mercy of fluctuations in the warm ionized ISM as well as turbulent structures (e.g., H II regions) which may lie along the line-of-sight. The dark bands that run through the approximate midpoint of Sh 2-216 (almost) completely depolarize the diffuse background emission. If Sh 2-216 were located $\sim 0.5^\circ$ south of its actual position, then the distinct signature of the north-east arc would be destroyed. Given the prevalence of turbulence in the ISM, this point is a significant concern. In fact, of the six PNe in the CGPS region known to interact with the ISM, only two, including Sh 2-216, are seen in polarization. (The other, namely DeHt 5, is the subject of a subsequent paper.) Targeted polarimetric observations of old PNe at sub-arcminute resolution and at multiple frequencies in the range 1–3 GHz are necessary to better establish the potential of these objects as good probes of the magnetized ISM.

5.2. A Stellar Origin for the Magnetic Field in the Shell of Sh 2-216

Can a $\sim 5 \mu\text{G}$ magnetic field in the interaction region be attributed to the host white dwarf near the center of Sh 2-216? The magnetic fields of white dwarfs have been measured via spectropolarimetric observations of optical absorption lines, but only recently have the observations had the sensitivity to detect kilogauss fields. The studies thus far have focused on either fully evolved (compact) white dwarfs (Aznar Cuadrado et al. 2004) or central stars of

relatively young PNe which are still transitioning to white dwarfs (Jordan, Werner, & O’Toole 2005). In the case of evolved white dwarfs, Aznar Cuadrado et al. (2004) found for a sample of 12 stars only three which had detectable magnetic fields in the range 2–4 kG, a detection rate of 25%. On the other hand, Jordan et al. (2005) found for each of a selection of four transition stars magnetic fields of 1–3 kG, a detection rate of 100%. Though the number statistics for both cases are relatively poor, this pair of results suggests that the magnetic fields of transition stars are present not in their degenerate cores but rather their extended envelopes, since magnetic flux is apparently lost during white dwarf evolution (i.e., during collapse from stellar radii in the Jordan et al. 2005 sample of $0.14\text{--}0.3 R_{\odot}$ to white dwarf radii of $\approx 0.012 R_{\odot}$). The magnetic fields of the central stars of old PNe have not been measured. Given their intermediate radius, e.g., $0.05 R_{\odot}$ for the “central” star in Sh 2-216 (based on the luminosity and effective temperature given in Rauch et al. 2007), measurements of the magnetic fields of the central stars of old PNe could lead to an improved understanding of field evolution in white dwarfs. We point out for completeness that a small fraction ($\sim 10\%$) of white dwarfs are observed to have magnetic fields at the 1 MG level or higher (see Liebert et al. 2003), but these stars tend to have masses ($\approx 0.9 M_{\odot}$) much higher than typical white dwarf masses ($0.48\text{--}0.65 M_{\odot}$), and may come from magnetized progenitors such as peculiar (Ap) stars (see Liebert 1988; Liebert et al. 2003).

For present purposes, we assume the magnetic field in the envelope around the contracting “central” star in Sh 2-216 to be accurately represented by the magnetic field ($B_{\text{avg}} = 1.8$ kG) measured at the radii ($r_{\text{avg}} = 0.21 R_{\odot}$) of the central stars in the Jordan et al. (2005) sample. With some knowledge of the large-scale magnetic field geometry, we can then estimate the field at large radii; namely, in the shell of Sh 2-216. Unfortunately, at this time, neither observations nor theory form a complete picture of the magnetic fields in PNe. Magnetic field measurements of maser spots in precursor (AGB) circumstellar envelopes suggest a radial dependence of the field ($B \sim r^{-2}$; see Vlemmings et al. 2002), while measurements for the supergiant VX Sgr show a poloidal dependence ($B \sim r^{-3}$; see Vlemmings, van Langevelde, & Diamond 2005). In contrast, the geometry of filamentary structures observed by Huggins & Manley (2005) in three PNe, as well as measurements by Vlemmings, Diamond, & Imai (2006) of the magnetic field structure in the jet emanating from AGB star W43A, suggest the dominance of toroidal fields ($B \sim r^{-1}$), consistent with the theoretical framework of Chevalier & Luo (1994). If either radial or poloidal geometries hold for Sh 2-216, then the magnetic field in the interaction region (≈ 1.0 pc from the host white dwarf) would fall well below our RM -estimated $\sim 5 \mu\text{G}$ line-of-sight field. On the other hand, if a toroidal field holds, then the magnetic field in the interaction region could be $\sim 8 \mu\text{G}$. Given the spherical symmetry of the shell of Sh 2-216, a large-scale toroidal magnetic field for this PN, invoked generally to explain non-spherical (e.g., bipolar, elliptical) symme-

tries in young PNe, is unlikely. However, localized enhancements of the internal magnetic field, due to compression in dense knots or filaments (see, e.g., Soker 2002; Soker & Kastner 2003), are possible. Thus we cannot completely dismiss the possibility of a $\sim 5 \mu\text{G}$ internal field in the shell of Sh 2-216. Detailed MHD simulations need to be done in order to better understand the magnetic field geometry in PNe.

6. CONCLUSIONS

Here we give a summary of our results and conclusions:

1. We presented 1420 MHz polarization images for the $2.5^\circ \times 2.5^\circ$ region in the CGPS around the PN Sh 2-216.

2. A low-polarized-intensity arc, $0.2^\circ \times 0.7^\circ$ in size, appears in the north-east portion of the visible disk of Sh 2-216. The arc is coincident with the optically-identified interaction region between the PN and the ISM.

3. A second low-polarized-intensity arc appears in the north-west portion of the visible disk of Sh 2-216.

4. The north-east arc contains structural variations down to the $\sim 1'$ resolution limit in both polarized intensity and polarization angle. Several polarization-angle “knots” appear along the arc.

5. Via comparison of the polarization angles at the centers of the knots in the north-east arc and the mean polarization angle outside Sh 2-216 (and above $b \simeq +0.5^\circ$), we estimated the RM through the knots to be $-43 \pm 10 \text{ rad m}^{-2}$.

5. Using this estimate for the RM and an estimate of the electron density in the shell of Sh 2-216, we derived a line-of-sight magnetic field in the interaction region of $5.0 \pm 2.0 \mu\text{G}$.

6. We believe it more likely the derived magnetic field is interstellar than stellar, though we cannot completely dismiss the latter possibility. We interpret our observations via a simple model which qualitatively describes the ISM magnetic field around Sh 2-216.

7. It is unclear whether old PNe like Sh 2-216 could be useful probes of the magnetized ISM. Targeted polarimetric observations at high resolution ($< 1'$), and possibly at multiple frequencies in the range 1–3 GHz, may help separate the signatures of more PNe from the turbulent ISM.

ACKNOWLEDGMENTS. We thank an anonymous referee for a constructive review

of the paper and for comments helpful in the preparation of the final manuscript. R.R.R. would like to thank Maik Wolleben for applying his Faraday screen model to our data and for insightful discussions. The Canadian Galactic Plane Survey is a Canadian project with international partners, and is supported by a grant from NSERC. The Dominion Radio Astrophysical Observatory is operated as a national facility by the National Research Council of Canada. This research is based in part on observations with the 100-m telescope of the MPIfR at Effelsberg. The Second Palomar Observatory Sky Survey (POSS-II) was made by the California Institute of Technology with funds from the National Science Foundation, the National Geographic Society, the Sloan Foundation, the Samuel Oschin Foundation, and the Eastman Kodak Corporation. The Wisconsin H-Alpha Mapper is funded by the National Science Foundation.

REFERENCES

- Aznar Cuadrado, R., Jordan, S., Napiwotzki, R., Schmid, H. M., Solanki, S. K., & Mathys, G. 2004, *A&A*, 423, 1081
- Bains, I., Bryce, M., Mellema, G., Redman, M. P., & Thomasson, P. 2003, *MNRAS*, 340, 381
- Beck, R., Brandenburg, A., Moss, D., Shukurov, A., & Sokoloff, D. 1996, *ARA&A*, 34, 155
- Beuermann, K., Kanbach, G., & Berkhuijsen, E. M. 1985, *A&A*, 153, 17
- Brown, J. C. & Taylor, A. R. 2001, *ApJ*, 563, L31
- Burn, B. J. 1966, *MNRAS*, 133, 67
- Chevalier, R. A. & Luo, D. 1994, *ApJ*, 421, 225
- Cudworth, K. & Reynolds, R. J. 1985, *PASP*, 97, 175
- Fosalba, P., Lazarian, A., Prunet, S., & Tauber, J. A. 2002, *ApJ*, 564, 762
- Gaensler, B. M., Dickey, J. M., McClure-Griffiths, N. M., Green, A. J., Wieringa, M. H., & Haynes, R. F. 2001, *ApJ*, 549, 959
- Ginzburg, V. L. & Syrovatskii, S. I. 1965, *ARA&A*, 3, 297
- Gray, A. D., Landecker, T. L., Dewdney, P. E., Taylor, A. R., Willis, A. G., & Normandeau, M. 1999, *ApJ*, 514, 221

- Haffner, L. M., Reynolds, R. J., Tufte, S. L., Madsen, G. J., Jaehnig, K. P., & Percival, J. W. 2003, *ApJS*, 149, 405
- Harris, H. C., Dahn, C. C., Canzian, B., Guetter, H. H., Leggett, S. K., Levine, S. E., Luginbuhl, C. B., Monet, A. K. B., Monet, D. G., Pier, J. R., Stone, R. C., Tilleman, T., Vrba, F. J., & Walker, R. L. 2007, *AJ*, 133, 631
- Haverkorn, M., Gaensler, B. M., Brown, J. C., Bizunok, N. S., McClure-Griffiths, N. M., Dickey, J. M., & Green, A. J. 2006a, *ApJ*, 637, L33
- Haverkorn, M., Gaensler, B. M., McClure-Griffiths, N. M., Dickey, J. M., & Green, A. J. 2006b, *ApJS*, 167, 230
- Haverkorn, M., Katgert, P., & de Bruyn, A. G. 2003a, *A&A*, 403, 1031
- . 2003b, *A&A*, 404, 233
- . 2004a, *A&A*, 427, 169
- . 2004b, *A&A*, 427, 549
- Heiles, C. 1996a, in *Astronomical Society of the Pacific Conference Series*, Vol. 97, *Polarimetry of the Interstellar Medium*, ed. W. G. Roberge & D. C. B. Whittet, 457–+
- Heiles, C. 1996b, *ApJ*, 462, 316
- Huggins, P. J. & Manley, S. P. 2005, *PASP*, 117, 665
- Jordan, S., Werner, K., & O’Toole, S. J. 2005, *A&A*, 432, 273
- Kerber, F., Mignani, R. P., Guglielmetti, F., & Wicenec, A. 2003, *A&A*, 408, 1029
- Kothes, R. & Landecker, T. L. 2004, in *The Magnetized Interstellar Medium*, ed. B. Uyaniker, W. Reich, & R. Wielebinski, 33–38
- Landecker, T. L., Dewdney, P. E., Burgess, T. A., Gray, A. D., Higgs, L. A., Hoffmann, A. P., Hovey, G. J., Karpa, D. R., Lacey, J. D., Prowse, N., Purton, C. R., Roger, R. S., Willis, A. G., Wyslouzil, W., Routledge, D., & Vaneldik, J. F. 2000, *A&AS*, 145, 509
- Landecker, T. L. et al. 2008, *AJ*, in preparation
- Liebert, J. 1988, *PASP*, 100, 1302
- Liebert, J., Bergeron, P., & Holberg, J. B. 2003, *AJ*, 125, 348

- Mathewson, D. S. & Ford, V. L. 1970, *MmRAS*, 74, 139
- Ng, T., Landecker, T. L., Cazzolato, F., Routledge, D., Gray, A. D., & Reid, R. I. 2005, *Radio Science*, 40, 5014
- Ohno, H. & Shibata, S. 1993, *MNRAS*, 262, 953
- Rand, R. J. & Kulkarni, S. R. 1989, *ApJ*, 343, 760
- Rand, R. J. & Lyne, A. G. 1994, *MNRAS*, 268, 497
- Rauch, T., Ziegler, M., Werner, K., Kruk, J. W., Oliveira, C. M., Vande Putte, D., Mignani, R. P., & Kerber, F. 2007, *A&A*, 470, 317
- Reich, P., Reich, W., & Fürst, E. 1997, *A&AS*, 126, 413
- Reid, R. I., Gray, A. D., Landecker, T. L., & Willis, A. G. 2008, *Radio Science*, 43, 2008
- Reynolds, R. J. 1985, *ApJ*, 288, 622
- Schnitzeler, D. H. F. M., Katgert, P., Haverkorn, M., & de Bruyn, A. G. 2007, *A&A*, 461, 963
- Soker, N. 2002, *MNRAS*, 336, 826
- Soker, N. & Dgani, R. 1997, *ApJ*, 484, 277
- Soker, N. & Kastner, J. H. 2003, *ApJ*, 592, 498
- Soker, N. & Zucker, D. B. 1997, *MNRAS*, 289, 665
- Spoelstra, T. A. T. 1984, *A&A*, 135, 238
- Taylor, A. R., Gibson, S. J., Peracaula, M., Martin, P. G., Landecker, T. L., Brunt, C. M., Dewdney, P. E., Dougherty, S. M., Gray, A. D., Higgs, L. A., Kerton, C. R., Knee, L. B. G., Kothes, R., Purton, C. R., Uyaniker, B., Wallace, B. J., Willis, A. G., & Durand, D. 2003, *AJ*, 125, 3145
- Tweedy, R. W. & Kwitter, K. B. 1996, *ApJS*, 107, 255
- Tweedy, R. W., Martos, M. A., & Noriega-Crespo, A. 1995, *ApJ*, 447, 257
- Uyaniker, B. 2004, in *The Magnetized Interstellar Medium*, ed. B. Uyaniker, W. Reich, & R. Wielebinski, 71–80

- Uyaniker, B. & Landecker, T. L. 2002, *ApJ*, 575, 225
- Uyaniker, B., Landecker, T. L., Gray, A. D., & Kothes, R. 2003, *ApJ*, 585, 785
- Vlemmings, W. H. T., Diamond, P. J., & Imai, H. 2006, *Nature*, 440, 58
- Vlemmings, W. H. T., Diamond, P. J., & van Langevelde, H. J. 2002, *A&A*, 394, 589
- Vlemmings, W. H. T., van Langevelde, H. J., & Diamond, P. J. 2005, *A&A*, 434, 1029
- Wareing, C. J., Zijlstra, A. A., & O’Brien, T. J. 2007, *MNRAS*, 382, 1233
- Wieringa, M. H., de Bruyn, A. G., Jansen, D., Brouw, W. N., & Katgert, P. 1993, *A&A*, 268, 215
- Willis, A. G. 1999, *A&AS*, 136, 603
- Wolleben, M., Landecker, T. L., Reich, W., & Wielebinski, R. 2006, *A&A*, 448, 411
- Wolleben, M. & Reich, W. 2004, *A&A*, 427, 537

Table 1. Polarization Angles in the “Knots” of the North-East Arc

Knot	$P.A.$ ($^{\circ}$) [1]	$\sigma_{P.A.}$ ($^{\circ}$) [2]	Extrema ($^{\circ}$) [3]	n [4]	$P.I.$ (K) [5]	$\sigma_{P.I.}$ (K) [6]
1	+33.6	13.4	+59.7, +21.0	10	0.139	0.017
2	+83.7	13.1	−74.4, +66.0	7	0.125	0.025
3	−88.1	4.2	−83.3, +86.8	10	0.122	0.013
4	+52.7	2.5	+55.6, +48.1	8	0.229	0.032
5	−79.9	2.4	−76.8, −84.3	10	0.175	0.015
6	−76.6	4.7	−70.2, −82.5	10	0.217	0.009
7	+89.9	3.9	−83.3, +84.9	10	0.187	0.016
8	+65.7	2.2	+69.7, +62.0	10	0.220	0.013

Note. — [1] Mean polarization angle over n pixels; [2] Standard deviation in polarization angle over n pixels; [3] Low, high value of polarization angle (running clockwise from $P.A. = 0$); [4] Number of pixels used to estimate the mean polarization angle; [5] Polarized intensity at center of knot; [6] Standard deviation in polarized intensity over n pixels. Polarization angles are modulo 180° ; i.e., angles of -90° and $+90^{\circ}$ are equivalent.

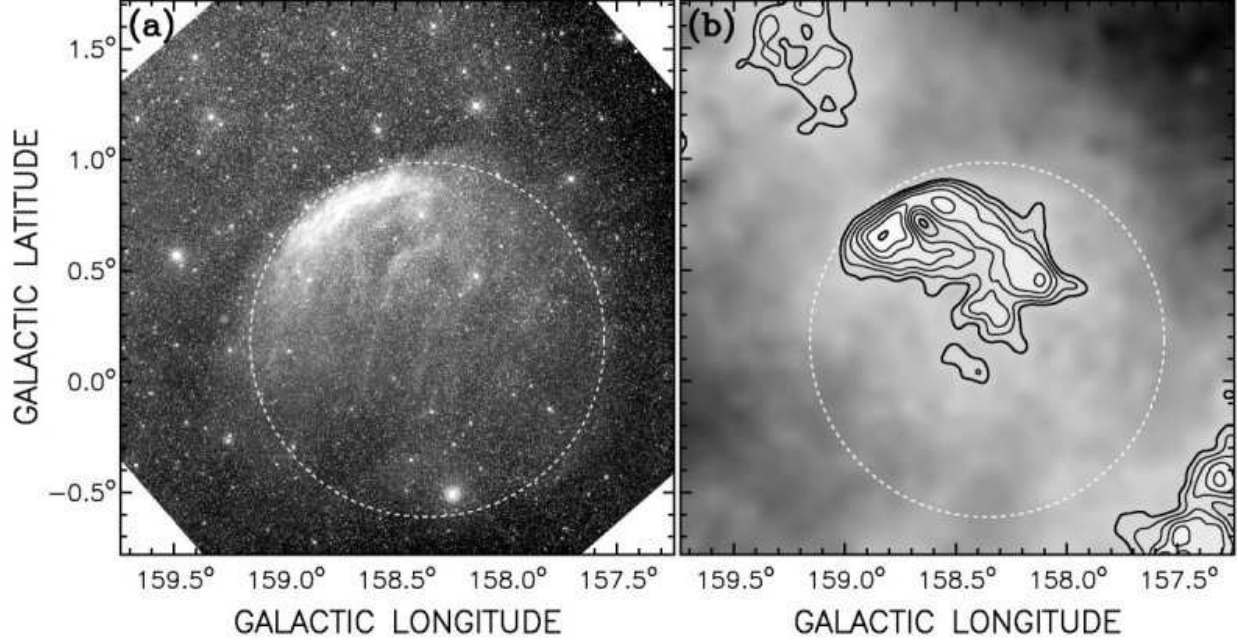


Fig. 1.— Images of the $2.5^\circ \times 2.5^\circ$ region centered approximately (see text) on the position of PN Sh 2-216 in (a) optical intensity at R-band (from the DSS) and (b) total radio intensity at 1420 MHz. Here and hereafter, images are presented in Galactic coordinates, with Galactic north up and Galactic east to the left. The gray scale is in photon counts in (a) and brightness temperature in (b), with lighter shades indicating higher counts/temperatures. The range of intensities in (a) has been adjusted to highlight extended emission. Point sources are removed in (b) leaving extended emission with brightness temperatures in the range 4.57–4.92 K. The contours drawn in (b) accentuate higher brightness temperatures, and run from 4.86 K to 4.92 K in steps of 0.01 K. The angular resolutions are (a) $\sim 1''$ and (b) $5'$ (smoothed from $\sim 1'$). The dotted circle drawn on each image, and on each subsequent image, shows the approximate extent of the visible disk of Sh 2-216.

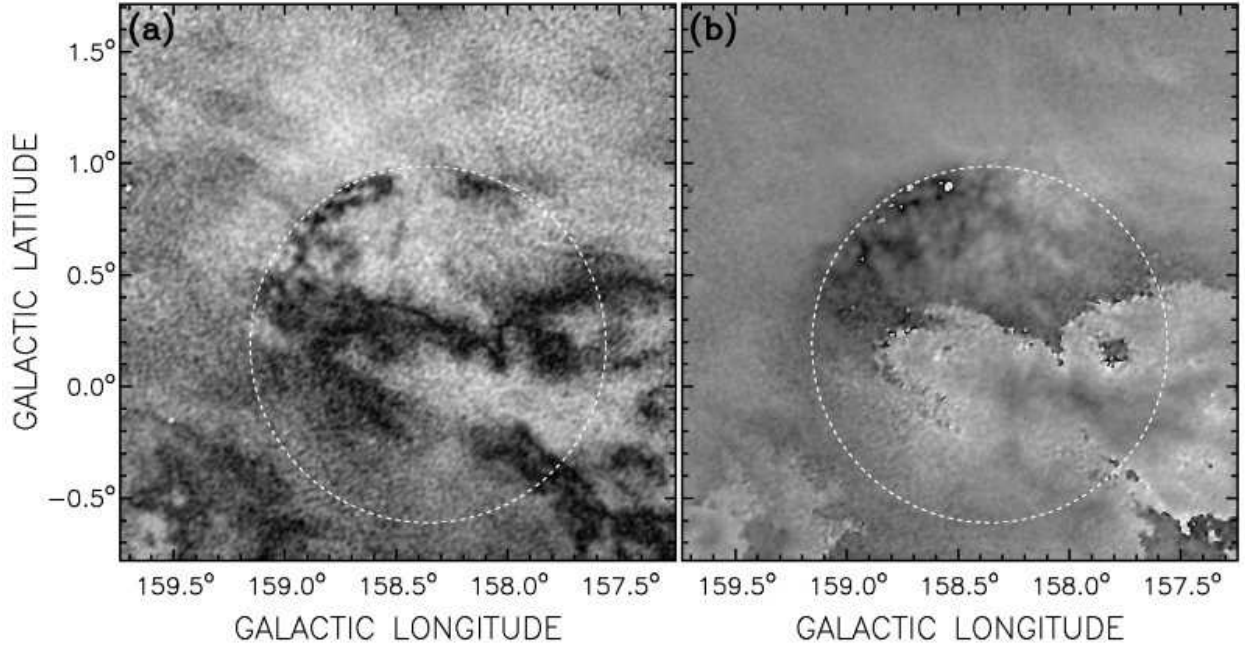


Fig. 2.— Images in (a) polarized intensity, $P = \sqrt{Q^2 + U^2 - (1.2\sigma)^2}$, and (b) polarization angle, $\theta_P = \frac{1}{2} \arctan U/Q$. The gray scale is in brightness temperature in (a) and runs from 0 to 0.67 K, with lighter shades indicating higher temperatures. The gray scale in (b) extends from -90° (black) to $+90^\circ$ (white). Note that abrupt black-to-white transitions in (b) do not represent large changes in angle, since polarization angles of -90° and $+90^\circ$ are equivalent. The resolving beam in each image is $1.31' \times 0.97'$ (full-width at half-maximum; FWHM) oriented at a position angle (east of north) of -40° .

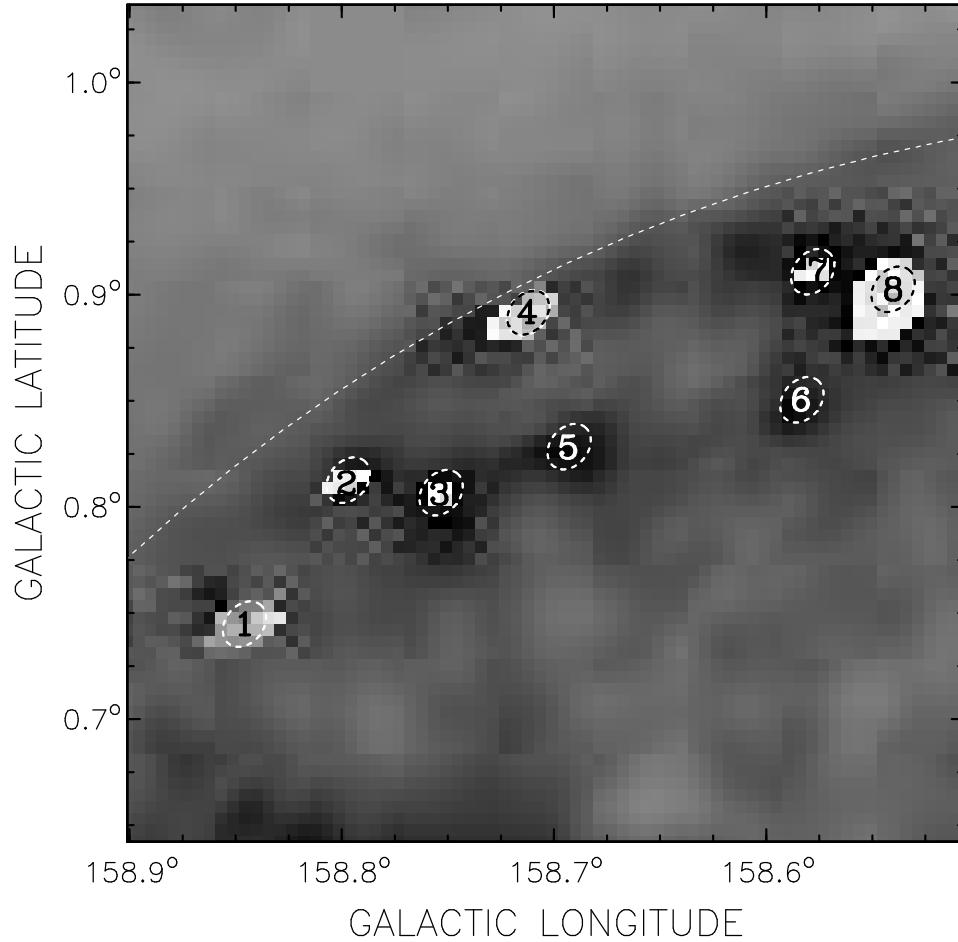


Fig. 3.— Polarization angle image zoomed to a $0.4^\circ \times 0.4^\circ$ region around the north-east arc. The gray scale is as described for Fig. 2*b*. The eight “knots” discussed in the text are labeled. The ellipses (thick dashed lines) drawn around each knot represent the resolving beam (FWHM), and define the knot perimeters for which the polarization angles (see Table 1) are determined.

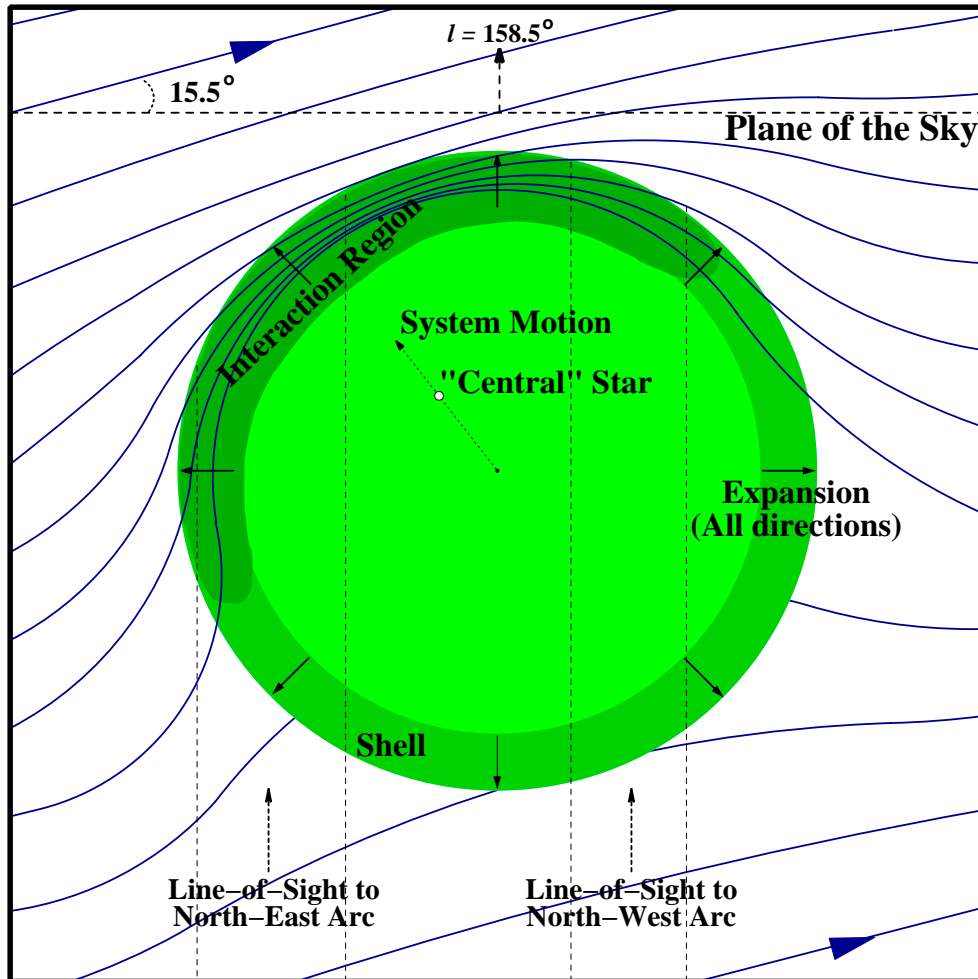


Fig. 4.— Simple model showing the interaction between Sh 2-216 and the ISM magnetic field. The perspective is that of an observer sitting above the Galactic plane and looking down on the center of the PN, with $l = 158.5^\circ$ directed upward. The PN is expanding in all directions. The motion of the PN system projected onto the Galactic plane is indicated. The host white dwarf (“central” star) is offset from the center of the PN toward the interaction region, where the ISM magnetic field (solid lines) is compressed and deflected around the shell of the PN. Magnetic field lines which appear to stop at the edge of the PN actually slide on the surface either above or below the slice shown. The intrinsic ISM field is inclined 15.5° to the plane of the sky. The lines-of-sight for an Earthbound observer to the north-east and north-west arcs are indicated.